Appl. Phys. B 65, 647–657 (1997)

Applied Physics B Lasers and Optics

Pulsed holmium laser ablation of tissue phantoms: correlation between bubble formation and acoustic transients

T. Asshauer[1], G. Delacrétaz[1], E.D. Jansen[2], A.J. Welch[2], M. Frenz[3]

[1] Institut d'Optique Appliquée, Ecole Polytechnique Fédérale de Lausanne, CH-1015, Lausanne, Switzerland
(Fax: +41-21-693 37 01, E-mail: guy.delacretaz@ioa.dmt.epfl.ch)
[2] Biomedical Engineering Program, University of Texas at Austin, Austin TX 78712, USA
[3] Institut für Angewandte Physik, Universität Bern, CH-3012 Bern, Switzerland

Received: 26 August 1996/Revised version: 10 February 1997

Abstract. Vapor bubble formation and related pressure transients during pulsed holmium laser ablation of tissues are suspected to induce damage. Poly(acrylamide) gels of 70–95 % water content with a Young's modulus of $0.14–4.6 \times 10^5$ Pa served as tissue phantoms to evaluate such effects. Holmium laser pulses (wavelength: 2.12 μm, duration: 180 μs FWHM), were delivered through 400 and 600 μm diameter optical fibers inserted into cubes of clear gel. Bubble effects were investigated using simultaneous flash micro-videography and pressure recording for radiant exposures of 20–382 J/cm^2.

Bubble formation and bubble collapse induced pressure transients were observed regardless of phantom stiffness. Bubbles of up to 4.2 mm in length were observed in gels with a Young's modulus of 2.9×10^5 Pa at a pulse energy of 650 mJ. An increase of Young's modulus (reduction in water content) led to a monotonic reduction of bubble size. In the softest gels, bubble dimensions exceeded those observed in water. Pressure amplitudes at 3 mm decreased from 100 ± 14 bars to 17 ± 6 bars with increasing Young's modulus over the studied range. Theoretical analysis suggested a major influence on bubble dynamics of the mass and energy transfer through the bubble boundary.

PACS: 42.62.Be; 62.50.+p; 87.45.-k

In many medical applications where laser energy is delivered via a fiber optic, the goal is the removal of tissue with minimal damage to surrounding tissue. Pulsed lasers are typically preferred to continuous wave lasers to minimize thermal damage [1]. Currently there is considerable interest in the holmium laser (Cr:Tm:Ho:YAG) at 2.12 μm because its wavelength is near the 1.94 μm absorption peak of water and is transmittable through standard low OH^- quartz fibers.

Holmium lasers are currently under investigation and in clinical use for a variety of applications. From a physical point of view, three groups of applications can be distinguished according to the laser-tissue interaction in different surroundings: (1) Ablation or coagulation of tissue in air, (2) Optical fibers positioned above a tissue surface in a liquid environment with pulses fired through the liquid towards the tissue surface and (3) The fiber tip is stuck into the soft tissue and laser pulses are fired while the tip is completely surrounded by tissue.

This study concentrates on experiments that model the last case. The experimental parameters mimic those used in clinical applications such as discectomy [2, 3] (intervertebral disc surgery) and vitrectomy [4] (surgery on the vitreous body of the eye).

Concerns have been raised about the extent of mechanical damage that may be produced by free-running holmium laser pulses (typically 200–350 μs duration). Dissections in vascular tissue during holmium laser angioplasty have been reported [5]. Expansion and collapse of a transient bubble formed in response to the laser irradiation has been suggested as the cause of the observed dissections [6]. Another cause of tissue damage is shockwave generation. Examples are mainly found during short pulse (ns-range) laser irradiations. Endothelial cell damage observed after Q-switched erbium laser irradiation of the cornea was attributed to the induced shockwaves [7]. Additionally, damage and killing of cells induced by shockwaves generated by short pulse lasers have been demonstrated in cell culture experiments [8, 9]. Strong mechanical effects are also reported during laser induced cavitation processes. Shockwaves induced at the collapse of bubbles generated by microsecond duration lasers are known to fragment kidney stones [10, 11].

Several groups have observed that pressure transients are produced during underwater free-running holmium laser irradiation [12, 13]. The mechanism of pressure generation is the collapse of a transient bubble induced by the laser pulse. As shown in a previous work [13], the pressure amplitudes can reach several thousand bars in water at the collapse center assuming a $1/r$ amplitude decrease of the spherically expanding pressure waves. At pulse energies associated with tissue ablation (fluence > 30 J/cm^2), a vapor bubble starts to form at the tip of the fiber typically 10 to 100 μs after the beginning of the laser pulse, depending on the fluence used [14, 15]. The bubble formation mechanism has been described by the Lausanne group as the explosive vaporization of an initially superheated volume of water [13]. The bubble grows to a maximum size typically in about 200 to 300 μs before collapsing [16].

The maximum bubble size is a function of the energy and the duration of the laser pulse [13]. Once sufficient energy is deposited to initiate vaporization, the laser radiation is transmitted through the expanding bubble and absorbed at the opposite side of the bubble. Long pulses ($> 100\,\mu$s) with fluences higher than 5 to 7 times the ablation threshold produce pear-shaped or even channel-like bubbles, as a result of the continuing vaporization process taking place after the initiation of the bubble [13].

In contrast, short pulses ($< 1\,\mu$s) always create a spherical bubble since all laser energy is deposited in the liquid water before a bubble forms, and thus the hydrodynamic process of bubble expansion and collapse does not interfere with the deposition of laser energy [17–19]. Regardless of the formation process, the collapse dynamics of long-pulse laser generated cavitation bubbles is similar to that created by short-pulse laser-induced cavitation as long as the bubble does not collapse before the end of the laser pulse [14]. The energy stored in the cavitation bubble is partially converted into acoustic energy at the collapse of the bubble, resulting in emission of an acoustic transient [20–22].

In this paper, we use poly(acrylamide) gel phantoms of different concentrations to examine the formation of vapor bubbles and acoustic transients in tissue by pulsed free-running holmium laser radiation. The size and dynamics of the bubbles formed in the gels are reported as a function of energy and fiber diameter and compared to those formed in water. Simultaneous pressure measurements allow us to correlate the occurrence of acoustic transients with the bubble dynamics.

1 Materials and methods

1.1 Poly(acrylamide) gel tissue phantoms

Poly(acrylamide) (PAA) gels were used as tissue phantoms. The PAA-gel water content was varied from 70–95 % to obtain tissue phantoms of various consistency. Unlike agar or gelatin, PAA-gel has excellent optical transparency for visible light and a melting point well above the boiling point of water [23]. The physical properties of an 85% water content PAA-gel are density $\varrho = 1.03\,\mathrm{g/cm^3}$, specific heat $c_p = 4.186\,\mathrm{Jg^{-1}K^{-1}}$, and thermal conductivity $k = 4.1 \times 10^{-3}\,\mathrm{Wcm^{-1}K^{-1}}$ [24].

Gels with water contents of 70% to 95% (corresponding to 30% to 5% PAA polymer content) were synthesized according to standard recipes [25] to model various tissue types. Gels with low PAA polymer concentrations (5–20 %) model soft tissues like the vitreous body of the eye, cornea, or liver, whereas gels with high polymer concentrations ($> 20\%$) model stiffer tissues like intervertebral discs or aorta. In order to allow a reasonable comparison with real tissue, the optical and mechanical properties of the gels were analyzed. Although PAA-gel models only partially represent tissues, which are more complex, they represent to our knowledge a reasonable transparent phantom for tissue.

1.2 PAA optical properties measurements

The absorption coefficients of the gels were measured from $2.08\,\mu$m to $2.22\,\mu$m. Values of μ_a were obtained from extinction measurements of 1.0 ± 0.01 mm thick gel samples using a spectrophotometer (Lambda 19, Perkin Elmer). The absorption curves for gels of 90% and 70% water content are compared to the water absorption curve in Fig. 1. Interestingly, the absorption coefficient at the holmium laser wavelength of $\lambda = 2.12\,\mu$m was almost constant and independent of the water contents. If the water molecules were the only absorber at this wavelength, a decrease of the absorption coefficient proportional to the water content would be expected, as actually observed for wavelengths below $2.1\,\mu$m (see Fig. 1). However, a PAA polymer absorption peak around $2.2\,\mu$m was observed. Due to the superposition of this polymer absorption band with the water absorption band around $1.94\,\mu$m there is a compensation effect at the $2.12\,\mu$m laser wavelength resulting in a almost constant absorption coefficient. This particular feature allows us to study the influence of the mechanical properties on bubble dynamics without having to take into account varying absorption properties. The measured absorption coefficient $\mu_\mathrm{a}(\lambda = 2.12\,\mu\mathrm{m})$ at room temperature (25 °C) is $25 \pm 0.5\,\mathrm{cm^{-1}}$.

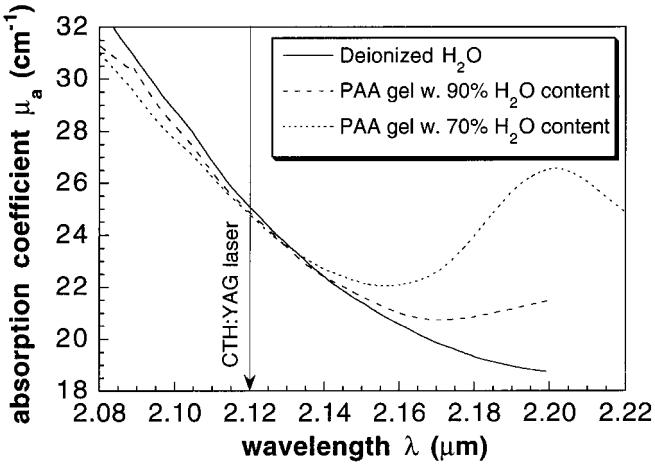

Fig. 1. Absorption coefficient μ_a of PAA-gels of 90% and 70% water content and of pure water as a function of wavelength

1.3 PAA mechanical properties measurements

The complete analysis of the dynamical response of PAA-gels at the high compression velocities reached during bubble expansion is a complex problem which is beyond the scope of this work. Here the viscoelastic response of the PAA-gels is investigated using the velocity range accessible with conventional material sciences testing techniques.

The gels are composed of a cross-linked network of PAA-polymer strands filled with a large amount of water (70 to 95% of weight). Such gels typically show viscoelastic behavior, i.e. their response to external stress comprises elastic (like a solid) as well as viscous (like a liquid) reactions [26]. The elastic modulus (or Young's modulus) E' of the gels as well as the viscous properties have been determined with a standard rheology measurement system (RSA II, Rheometrics, USA).

Cylindrical gel samples of 14 mm diameter and $z = 8$ mm thickness were mounted between two pistons. A precompression static load of 30 g was applied to insure a good mechanical contact. The viscoelastic response of the sample was analyzed in two experiments:

Table 1. Young's modulus of poly(acrylamide) (PAA) gels under slow dynamic compression (0.8 mm/s)

Water content (%)	Polymer content (%)	Young's Modulus $E'/10^5$ Pa
95	5	0.142 ± 0.008
92	8	0.43 ± 0.05
90	10	0.83 ± 0.06
84	16	2.45 ± 0.13
80	20	2.87 ± 0.15
70	30	4.6 ± 0.3

(a) The sample was compressed until rupture at a constant strain rate of $0.2\,\mathrm{s}^{-1}$ (rate of relative thickness change $\partial/\partial t \cdot \Delta z/z$), which corresponds to a piston speed of 1.6 mm/s for a sample of $z = 8$ mm thickness. The Young's modulus is given by the slope of the exerted force versus strain plot; the values obtained at a strain of -0.25 (compression to 75% of the original thickness) for gels of each PAA concentration are reported in Table 1. The Young's modulus increases with increasing polymer content (decreasing water content) as expected from elasticity theory [27].

(b) The dynamic variation of the Young's modulus was derived using a conventional method [28], from the dynamic response of samples submitted to a sinusoidal compression force $\sigma_t = \sigma_0 \sin \omega t$ characterized by a maximal strain $\varepsilon = \Delta z/z$ of 0.05. The investigated stress frequencies were between 1 and 100 rad/s. The maximum stress frequency (limited by the instrument) corresponded to a maximum velocity of 40 mm/s. This represents a velocity three orders of magnitude lower than the speed reached during the bubble expansion phase (10 m/s). However we will assume that no singularity in the viscoelastic response exists at high speed, and thus that the viscoelastic comportement observed at low velocity can be extrapolated to high frequencies.

As the gels behave viscoelastically, the deformation of the gels in response to the sinusoidal stress σ_t experiences a delay [29, 30]: $\varepsilon_t = \varepsilon_0 \sin(\omega t - \theta)$. The mechanical properties are described by the complex modulus $E^* = E' + \mathrm{i}E'' = \sigma_0/\varepsilon_0 \cos\theta + \mathrm{i}\sigma_0/\varepsilon_0 \sin\theta$. The first component, the Young's modulus E', describes the strain in phase with the applied stress, while the second component E'' describes the strain 90* out of phase. E'' characterizes the loss of mechanical energy by dissipation into heat in the gel, it is commonly referred to as the loss modulus.

Figure 2 shows the frequency dependency of E' and E'' for PAA-gels of 95% and 80% water content. Only a slight increase of the Young's modulus E' with the excitation frequency was measured. The loss modulus E'' was more than an order of magnitude smaller than E' for both gels, indicating that the elasticity is dominant over viscous effects. In the 80% water content gel, a maximum of E'' (1.0×10^4 Pa) was measured at a compression frequency of 2.2 rad/s. For higher frequencies the loss modulus decreased. For the 95% water content gel, a monotonic decrease of E'' was observed over the measured frequencies.

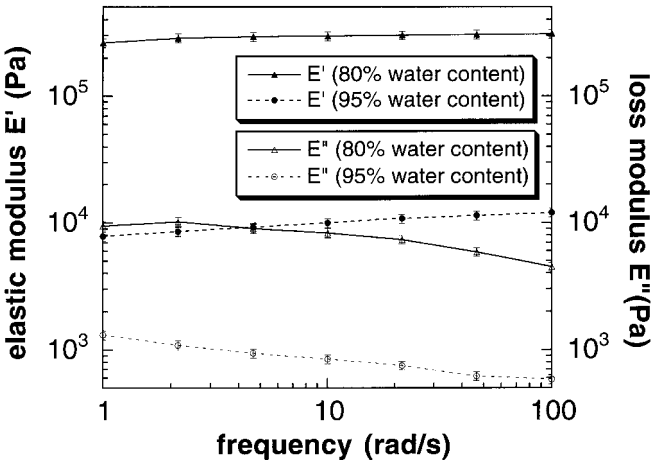

Fig. 2. Rheology measurements of elastic modulus E' and loss modulus E'' of PAA-gels of 95% and of 80% water content as a function of compression frequency. PAA disks of 14 mm diameter and 8 mm thickness were compressed in thickness by sinusoidal forces of an amplitude resulting in a maximum strain of 5%

1.4 Bubble dynamics and pressure measurements experimental setup

The experimental setup used for the bubble dynamics and pressure measurements is schematically represented in Fig. 3. The free running holmium laser (Cr:Tm:Ho:YAG) with a wavelength of 2.12 μm was operated at a pulse duration of 180 μs full width at half maximum (FWHM), corresponding to a total pulse duration of 250 μs. The pulse to pulse stability of the laser energy was better than 2%. Laser pulses were delivered to the target by low OH^- quartz fibers with core diameters of 400 and 600 μm. The fiber tip was gently inserted in the center of a PAA-gel sample of 2 cm × 2 cm × 2 cm, in order to induce minimal constraint during introduction of the fiber. Each PAA-bloc was placed on a platform in a 10 cm × 10 cm × 10 cm glass container filled with deionized water. Generally gels of 85 to 95% water behaved like a fluid when the fiber was inserted, while some tearing occured for lower water content. Control experiments were performed with the fiber tip placed in deionized water without the gel.

Two series of experiments were performed to study the bubble dynamics and pressure transient generation for the two

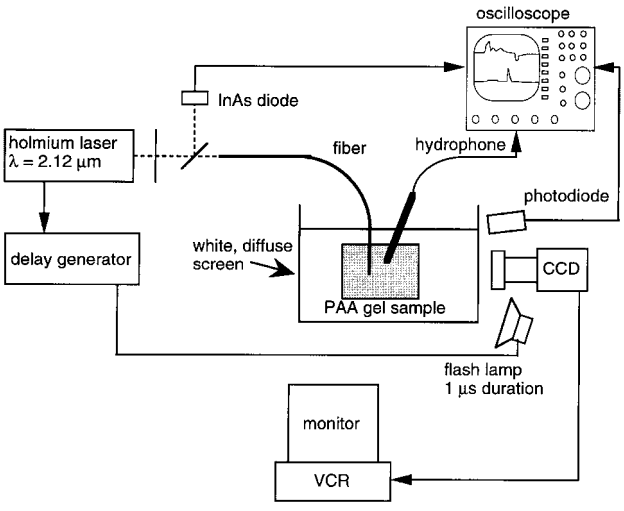

Fig. 3. Experimental setup

fiber diameters as a function of gel water content (70% to 100%) and as a function of fluence. In the first series, the gel water content was varied and the laser pulse energy delivered at the tip of the fiber fixed at 480 mJ, corresponding to fluences of $170 \pm 3\,\mathrm{J/cm^2}$ and $382 \pm 7\,\mathrm{J/cm^2}$ with the 600 μm and 400 μm fibers, respectively. In a second series of measurements, the fluence was varied from 20 to $230\,\mathrm{J/cm^2}$ using a 600 μm core diameter fiber and gel samples of 80% water content. A fresh sample was used for each laser shot.

The bubble formation was observed by time resolved flash videography. A xenon strobe lamp illumination source (Hamamatsu, Japan) with a 1 μs duration was used to illuminate the fiber tip. A white diffusing screen was placed behind the water container (see Fig. 3). The combination of direct and indirect illumination provided images where the whole bubble was visible as a three-dimensional object rather than its outline as in conventional shadow photography. Even the inside of the bubble was visible to some extent, providing additional information on the processes involved. Images were taken with a monochrome CCD camera (FK 6990, Cohu, USA), fitted with a 35 mm camera macro-zoom objective which allowed a working distance of 5–6 cm with a depth of focus of several millimeters. The holmium laser, the CCD camera frames and the strobe lamp were synchronized via a digital delay time generator (DG 535, Stanford Research Systems, USA). Time delays of 0 to 1000 μs between the beginning of the laser pulse and the strobe flash could be chosen. The observed error in the time delays of 1 μs was due to the ignition jitter of the laser flash lamp.

The pressure profile associated with each bubble event was recorded with a polyvinylidene difluoride (PVDF) needle probe hydrophone (Imotec, Germany) with an active zone diameter of 0.5 mm. The needle probe hydrophone was slowly moved into the gel block with its axis pointing in the direction of the expected origin of acoustic transients (location of bubble collapse) up to a distance of 3 to 4 mm; thus it was positioned well outside the maximum bubble radius, preventing any disturbance of the bubble dynamics (see Fig. 3). In order to compare the strength of the pressure transients from different experiments, the recorded pressures were normalized to a standard distance of 3 mm assuming that the acoustic transients propagate from their origin at the bubble collapse center as spherical waves [21] and thus the peak pressure decays like $1/r$. The distance from the hydrophone to the collapse center was measured on video images; the error in the distance measurement is less than 0.2 mm. Ten measurements were performed for each set of parameters.

The rise time of the hydrophone (10–90 %) was specified at $\tau_\mathrm{r} = 50$ ns. This limited rise time can lead to an underestimation of the actual peak pressure if the duration of the acoustic transient is shorter than τ_r. The measured peak pressures were therefore corrected using a method described previously [31] which accounts for the duration of the observed pressure transients. The pressure transient duration was experimentally determined by analysis of high magnification shadow photographs of pressure fronts obtained by illuminating with Nd:YAG laser pulses of 5 ns duration in a separate experimental setup.

A single laser pulse was delivered in each gel sample, once the optical fiber and pressure transducer were placed at a given location. The resulting acoustic transient and a single picture of the induced bubble at a specific delay time were recorded. The process was repeated with new gel samples for each investigated imaging time and for all laser parameter settings.

2 Results

2.1 Bubble dynamics and pressure transients in PAA-gel

The dynamic behavior of bubbles generated by holmium laser irradiation of PAA-gels of 95 to 70% water content has been investigated and compared to that observed in deionized water. Images of the characteristic bubble evolution recorded in gels of 95 and 80% water content and in pure water are shown in Fig. 4. For this series, the fiber core diameter was 600 μm, the laser pulse duration 180 μs (FWHM) and the energy was 480 mJ, resulting in a fluence of $170\,\mathrm{J/cm^2}$ at the fiber tip.

Bubbles observed for PAA-gels of high water content (95 and 92%) exhibit mostly spherical to slightly pear-shaped forms. An example of a bubble formed in a gel of 95% water content is shown in Fig. 4a. An irregularly structured surface appearance is often seen for the larger bubbles formed in gel of high water content. Increasing the PAA content of the gel, that is increasing its elastic modulus E', hinders the expansion process of the bubble, leading to a reduction of the maximal bubble size and accordingly of the bubble lifetime as illustrated in Fig. 4b for the 80% water gel. Size reduction is accompanied by a decrease in symmetry of the bubble, which appears more and more elongated and distorted. Moreover, bubbles formed in gels of the higher PAA concentration exhibit strongly perturbed symmetry at collapse [Fig. 4b, 300 μs image].

Interestingly, the maximal bubble sizes observed in pure water, which are in agreement with bubble dynamics reported previously by our group [13, 32] are smaller than the maximal sizes recorded in 95% water content gels [compare Figs. 4a,c]. Accordingly, bubbles formed in these gels also last longer than bubbles formed in water.

The characteristic dimensions (maximum diameter and length) of the bubbles observed at all investigated PAA concentrations for the same laser parameters as in Fig. 4 are reported in Fig. 5. The symbols represent the mean of the measured quantities with error bars representing the standard error, as in all subsequent graphs. The difference in the size of bubbles formed in pure water (100%), as compared to those of bubbles in gels of 95 and 92% water content, can be clearly seen. The maximum forward length of the bubbles, that is their maximum extension into the medium beyond the tip of the fiber (as opposed to the total of their forward and backward lengths), is also shown in Fig. 5. A maximal forward length of 3.2 mm is reached in the softest gel (95% water content). This value decreases with increasing gel stiffness to 1.6 mm for a gel with 70% water content. Note also that the ratio of forward extension to total length is greater in soft gels and water (about $2/3$) than in stiffer gels where it approaches $1/2$.

The threshold fluence at which bubbles form as a function of the gel PAA content has been investigated. In the irradiation conditions of bubbles presented in Figs. 4 and 5, i.e., with a fiber diameter of 600 μm and a pulse duration of 180 μs the threshold fluence necessary to initiate

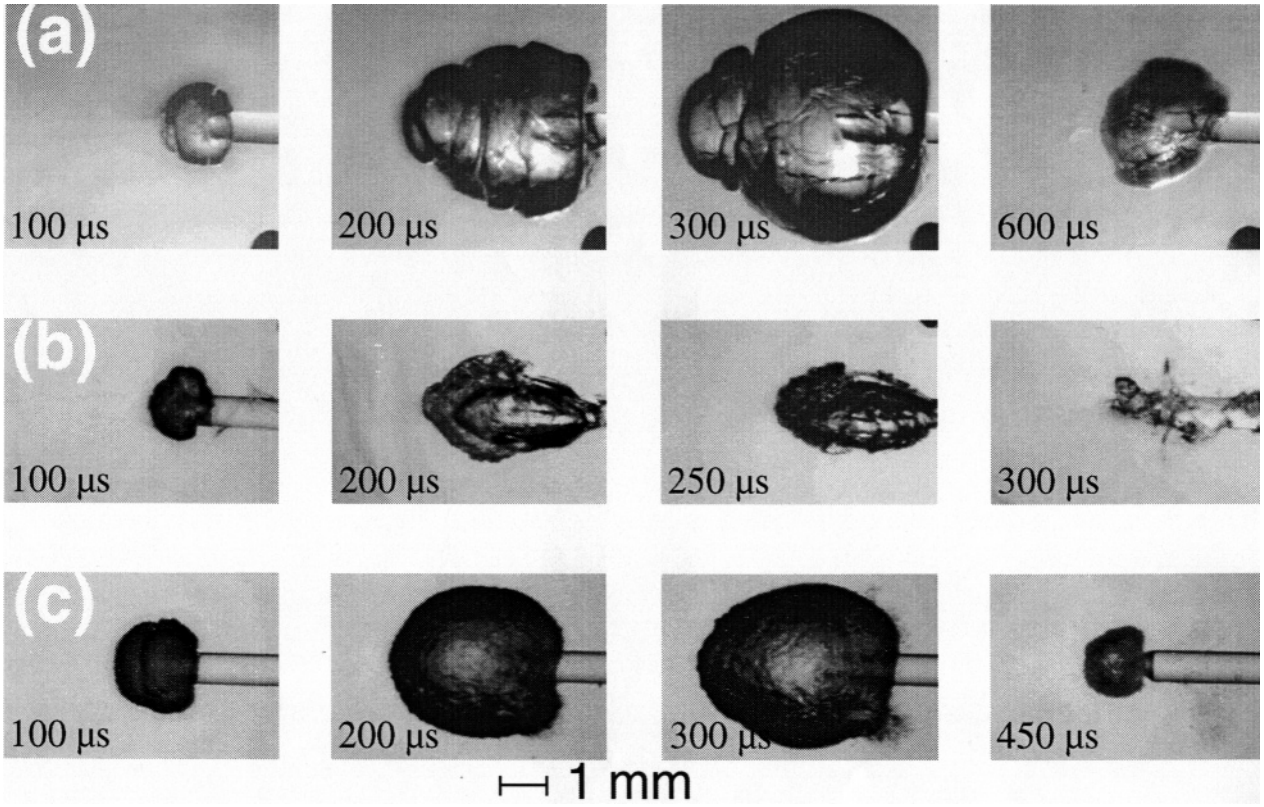

Fig. 4a–c. Strobe images of bubble dynamics in water and PAA-gels created by 480 mJ pulse energy with a duration of 180 µs (FWHM). Fiber core diameter 600 µm, resulting in a fluence of 170 J/cm^2 at the fiber tip. **a** 95% water content PAA-gel. **b** 80% water content PAA-gel. **c** Deionized water

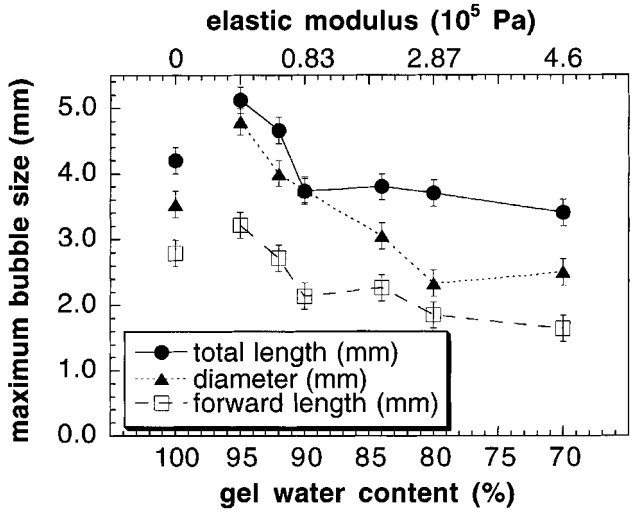

Fig. 5. Maximum diameter, maximum total length and maximum forward length (from fiber tip) of bubbles as a function of gel water content and elastic modulus. The 100% gel water content points represent pure water. Pulse energy 480 mJ, fiber core diameter 600 µm radiant exposure 170 J/cm^2, pulse duration 180 µs (FWHM)

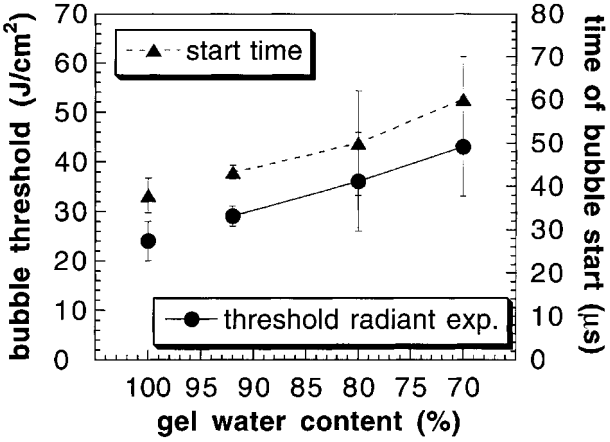

Fig. 6. Threshold radiant exposure for bubble formation and time delay between the beginning of the laser pulse and the start of bubble formation as a function of gel concentration for a fiber core diameter of 600 µm. Pulse duration 180 µs (FWHM)

bubble formation increased from 24 ± 4 J/cm^2 in pure water to 43 ± 10 J/cm^2 for the 70% water content gel (Fig. 6). Similarly, for a constant fluence of 170 J/cm^2, the delay between the start of the laser pulse and the onset of bubble formation increases from 38 ± 4 µs to 60 ± 10 µs, as more time is needed to deposit the energy density necessary to reach the higher threshold fluence in low water content gels. Note that the bubble formation thresholds observed, imply temperatures exceeding 100 °C prior bubble formation, that is superheating of the gel or water layer next to the fiber tip.

Some typical examples of pressure transients associated with the collapse of the bubbles imaged and documented above are shown in Fig. 7. The characteristic features reported in water [13] are also observed in gels. The major pressure transient occurs at the first collapse of the cavitation bubble, some hundreds of microseconds after the laser irradiation started (Fig. 7). This transient is followed by weaker pres-

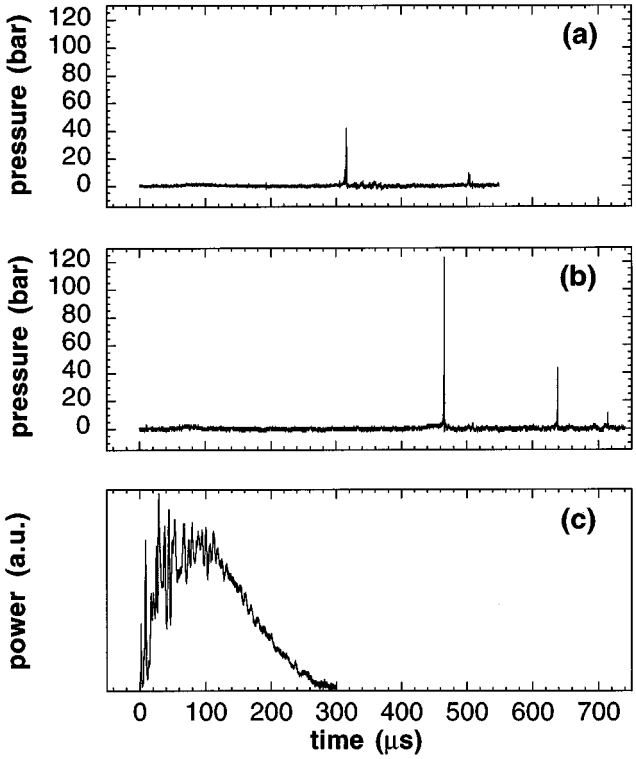

Fig. 7a–c. Time profile of pressure transients induced by 480 mJ pulses (radiant exposure 170 J/cm^2) at 3 mm distance in: 80% water content PAA-gel (**a**), and deionized water (**b**). Temporal profile of the laser pulse (**c**); Pulse duration 180 μs (FWHM)

sure transients associated with subsequent bubble collapses and rebounds . Only a relatively weak (below 5 bars) pressure rise is observed at the bubble onset during the laser pulse [13].

As an example, two pressure transients recorded in an 80% water content gel (Fig. 7a) and in water (Fig. 7b) after irradiation by a 480 mJ and 180 μs (FWHM) duration laser pulse (Fig. 7c) are shown. Note the hindered bubble expansion in the 80% water gel leading to a reduced bubble lifetime, a weaker bubble oscillation after the collapse and weaker pressure transients. Only the positive (compressive) part of the pressure transient induced at the bubble collapse is of high amplitude. The negative tail of the transient, weak and long lasting, is not seen.

The effect of the fiber diameter (600 and 400 μm) on the bubble geometry can be seen in Fig. 8. The bubbles induced in a PAA-gel of 90% water content and in pure water by a laser pulse of 480 mJ are shown at their maximum extension. Due to the smaller diameter of the 400 μm fiber, which leads to a 2.25 times higher fluence at its tip as compared to that of the 600 μm fiber, a more elongated (pear-shaped) bubble is formed with the 400 μm fiber. Thus, at the same pulse energy a deeper forward extension is observed for the smaller fiber diameter.

The influence of fiber diameter as well as of elastic modulus (PAA content) on the amplitude of the major acoustic transient induced by the bubble collapse (normalized to a distance of 3 mm from the fiber tip) is shown in Fig. 9 for constant pulse energy. The strength of the acoustic transient decreases with increasing PAA content of the gels. This effect correlates with the decrease in the bubble lifetime (Fig. 10) and in the maximal bubble size (Fig. 5). In pure water, stronger pressure

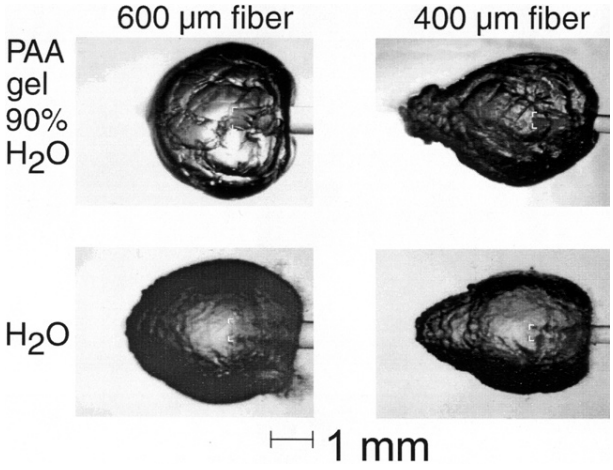

Fig. 8. Effect of fiber diameter on bubble geometry at maximum size in PAA-gel of 90% water content and in pure water. Energy 480 mJ, pulse duration 180 μs (FWHM). Left column: fiber core diameter 600 μm, radiant exposure 170 J/cm^2. Right column: fiber core diameter 400 μm radiant exposure 382 J/cm^2. The white symbols indicate the fiber tip position

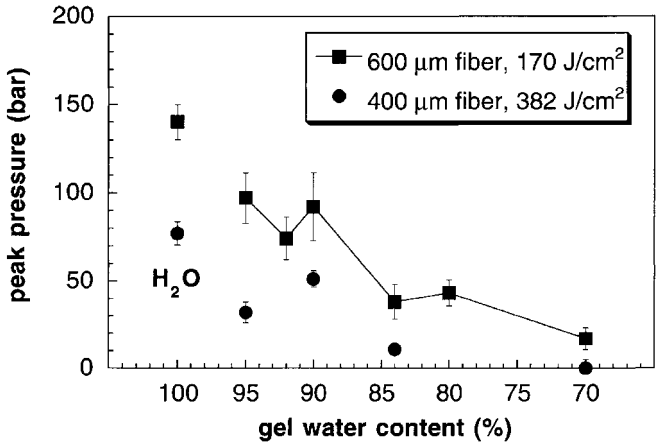

Fig. 9. Pressure amplitudes induced by the first bubble collapse at 3 mm distance from the collapse center as a function of gel water content for different radiant exposures and fiber diameters; energy 480 mJ, pulse duration 180 μs (FWHM). (■) Fiber core diameter 400 μm radiant exposure 382 J/cm^2. (●) Core diameter 600 μm radiant exposure 170 J/cm^2

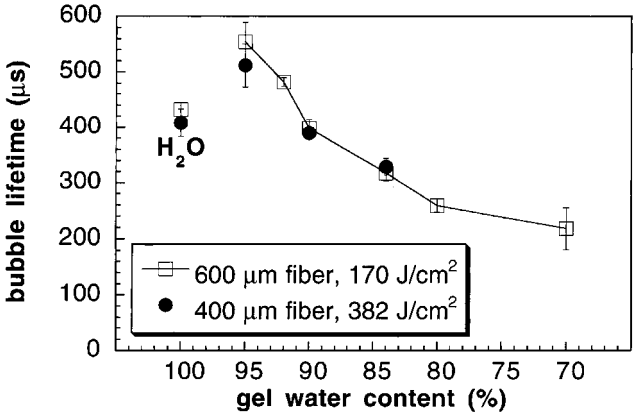

Fig. 10. Bubble lifetime (time from bubble start to first collapse) as a function of gel water content for different radiant exposures and fiber diameters; energy 480 mJ, pulse duration 180 μs (FWHM). (●) Fiber core diameter 400 μm radiant exposure 380 J/cm^2. (□) Core diameter 600 μm radiant exposure 170 J/cm^2

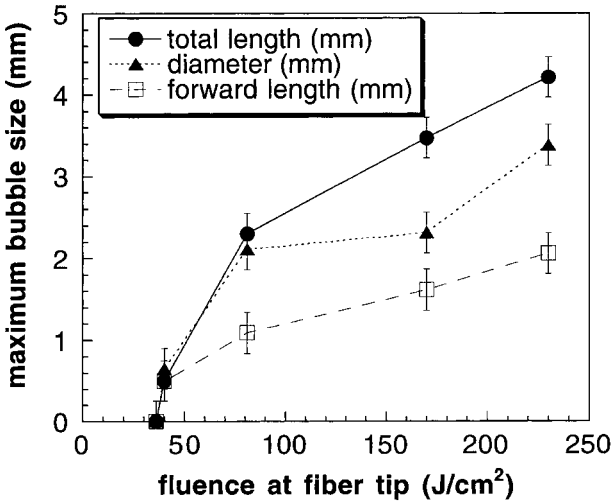

Fig. 11. Maximum bubble dimensions (diameter, total length and forward length) as a function of laser fluence at the fiber tip in 80% water content PAA-gel. Pulse duration 180 μs (FWHM), fiber core diameter 600 μm

transients than in any gel are generated at both fluences; however, the larger bubbles are produced in the gels of 95 and 92% water content.

For the same pulse energy, pressures were lower with the 400 μm fiber by at least a factor 2 in all gels. For both fluences, a reduction of the pressure by a factor 3 to 4 is observed for the higher PAA content gels as compared to pure water. The highest pressure observed in the gel was 100 ± 14 bars at 3 mm distance in the 95% water content gel with the 600 μm fiber. In the stiffer gel with 70% water content, the peak pressures dropped to 17 ± 6 bars for the 600 μm fibers and below 5 bars for the 400 μm fibers.

The effect of the fluence on the maximal size of the bubbles and on the pressure generated at their collapse was investigated for the 80% water content gel, which has a Young's modulus of $2.87 \pm 0.15 \times 10^5$ Pa and the largest fiber diameter (600 μm).

The dimensions of the bubbles at the moment of their maximal size are shown in Fig. 11 as a function of the fluence. Maximal total bubble length and lateral extension increased rapidly for fluences above the threshold of 36 ± 10 J/cm^2. For higher fluences, the length tended to increase faster than the lateral extension. At the highest fluence used (230 J/cm^2, corresponding to 650 mJ energy), bubbles of up to 3.4 mm in lateral extension and 4.2 mm length were observed. The forward length of the bubble was slightly smaller than the backward length for all fluences (Fig. 11). This is caused by the weakening of the gel around the fiber due to the channel created by pushing the fiber into the gel block.

The amplitude of the pressure transients associated with the bubbles is reported in Fig. 12, as well as the bubble lifetime for increasing fluence. A steady increase of the induced peak pressure is observed for fluences above the threshold, up to 58 ± 7 bars at 3 mm distance at the maximal investigated fluence of 230 J/cm^2.

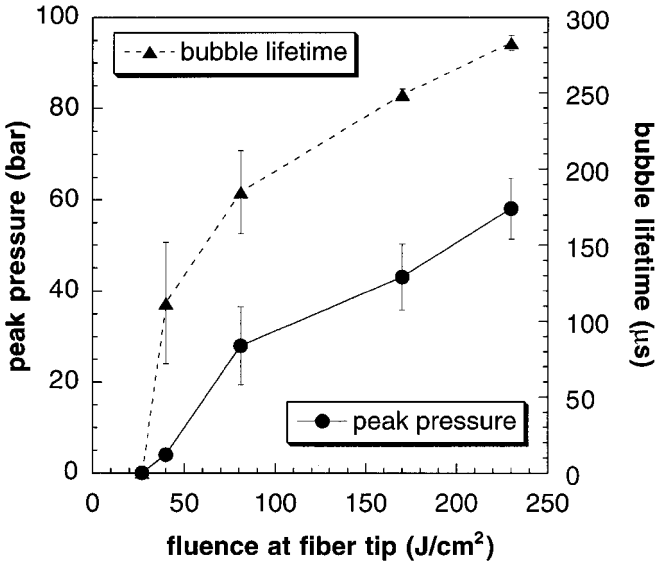

Fig. 12. Bubble lifetime and collapse pressure amplitudes as a function of laser radiant exposure in 80% water content PAA-gel. Pulse duration 180 μs (FWHM), fiber core diameter 600 μm

3 Discussion

The use of PAA-gels of different water content as tissue phantoms allowed us to mimic biological tissues of differing properties, ranging from very soft tissue, like the vitreous body of the eye, to tissue of relatively hard consistency like intervertebral discs (see Tables 1 and 2). Although they can be considered as far from tissue in terms of homogeneity and specific microscopic architecture, PAA-gels represent more realistic representations of tissue than water and gelatin due to their polymer structure. In particular PAA-gels melt at a temperature above the water boiling temperature, contrary to gelatin, a tissue model frequently used in previous studies of laser-tissue interactions.

Holmium laser irradiation at the investigated fluences, which compare or are even lower than that typically used in clinical applications, generates large vapor bubbles in all investigated phantoms, that is for material having a Young's modulus between 0.14×10^5 and 4.6×10^5 Pa. Although a steady decrease in the bubble size is observed for increasing PAA content (increasing Young's modulus), significant vapor bubble sizes of several millimeters in diameter (Figs. 5 and 12) have been observed even for the stiffer samples (70–80 % water content), having a Young's modulus of 2.9×10^5 to 4.6×10^5 Pa.

The amplitude of the induced acoustic transients is reduced with increasing phantom stiffness. Pressure transient

Table 2. Young's modulus and water contents of some real tissues

Tissue	Water content (%)	Young's Modulus $E'/10^5$ Pa
vitreous body [4]	98	
cornea	80	
vertrebal discs		
nucleus pulposus [44, 45]	85	< 3
lateral annulus [44, 45]	78	3–7
meniscus [46]		4.1
articular cartilage [46]	65–75	5–9

generation is quite strongly perturbed by the resistance of the gel polymer structure; pressure transients reaching up to 60 bars at three millimeters distance in gel with a Young's modulus of 2.9×10^5 Pa have been measured. Bubble dimensions, lifetime and collapse pressure all decrease with increasing gel stiffness at constant energy (Figs. 5, 10 and 9, respectively). The pressure amplitude decrease is particularly pronounced. Analogous to our previous observations in water [13, 32], the geometry of the bubble has an important influence on the collapse pressure generation. With increasing fluence, the bubble shape deviates from spherical symmetry to a more and more elongated pear shape. In the stiffer gels, the bubbles become more and more elongated with even more complex shapes than in water. Accordingly, a large decrease in pressure amplitude is observed due to the asymmetry of the bubble collapse in these gels. Similarly it is expected that in real tissues of much lower homogeneity, presenting various interfaces, like arterial walls, even stronger bubbles asymmetries will be induced, thus decreasing the strength of the pressure transients generated.

Although a decrease of the bubble dimensions is observed for increasing tissue phantom stiffness, the direct comparison with the cavitation activity generated in pure water indicates that cavitation in gels or tissue is a more complex process than in water. Indeed the maximal bubble extension in tissue is the result of the competition between several effects, mainly mechanical resistance and thermal energy transfer through the bubble boundary (heat conduction and condensation). This is particularly well illustrated by the surprising larger bubble sizes observed in gels of low PAA content, as compared to those formed in pure water (Figs. 4 and 5).

A qualitative analysis of the system of equations governing the bubble dynamics allows us to describe possible origins of this effect. The description of bubble dynamics far out of thermodynamic equilibrium in arbitrary media is a complex problem for which solutions have so far only been obtained for special cases involving simplifying assumptions, like spherical symmetry and ideal gas and liquid behavior. Using simplified equations allows us to discuss qualitatively the contribution of different physical phenomena to the bubble dynamics, in particular the maximal bubble extension and collapse induced pressure.

The dynamics of a spherical bubble in an infinite viscous liquid can be described by the Rayleigh-Plesset equation of motion [33]:

$$R\ddot{R} + \frac{3}{2}(\dot{R})^2 = \frac{1}{\varrho_\mathrm{l}}\left(p_\mathrm{i} - p_\infty - \frac{2\sigma}{R} - \frac{4\eta}{R}\dot{R}\right), \tag{1}$$

where R[m] is the bubble radius, ϱ_l[kg/m^3] is the density of the liquid phase, p_i[Pa] and p_∞ are the pressures at the interface and at infinity, respectively, σ[N/m] is the surface tension and η[Pa s] the viscosity of the liquid. $\dot{R}$ is the velocity and $\ddot{R}$ the acceleration of the bubble boundary.

The forces driving the motion of the liquid or gel surrounding the bubble are mainly generated by the pressure difference $\Delta p = p_\mathrm{i} - p_\infty$ (Eq. (1)). In its expansion phase, the bubble is filled with water vapor at a pressure above the ambient pressure ($\Delta p > 0$) that pushes the surrounding medium outward. When Δp becomes negative, bubble expansion decelerates until the kinetic energy of the liquid is consumed, then the collapse stage begins. The third and fourth terms on the right side of (1) represent additional forces necessary to overcome the surface tension and the viscosity. As they are inversely proportional to the bubble radius R, their relative influence decreases rapidly with increasing bubble size.

To describe bubble dynamics in gels, an additional term $f(E', R)$, which accounts for the force due to elastic material deformation, has to be added in the equation of motion. The bubble wall equation of motion is then:

$$R\ddot{R} + \frac{3}{2}(\dot{R})^2 = \frac{1}{\varrho_\mathrm{l}}\Bigg(p_\mathrm{i}\big(V, m_\mathrm{v}, T(\boldsymbol{r})\big) - p_\infty - \frac{2\sigma}{R} - \frac{4\eta}{R}\dot{R} - f(E', R)\Bigg). \tag{2}$$

For an ideal elastic solid, the term $f(E', R)$ is a monotonically increasing function of E' and R. From (2) it can be seen that increasing material viscosity, η, or elastic modulus, E', leads to a decrease in the speed of bubble expansion and maximal size. This observation is in agreement with the measured decrease in maximum bubble dimensions for a given laser energy with increasing elastic modulus (see Fig. 5). The local vapor pressure $p_\mathrm{i}(V, m_\mathrm{v}, T(\boldsymbol{r}))$, depending on the bubble volume V, the vapor mass m_v and the local temperature $T(\boldsymbol{r})$ via an equation of state, couples the hydrodynamic equation of motion to the thermodynamic processes of vapor generation and condensation.

In contrast to short pulse laser-induced cavitation, a water vapor source term has to be incorporated in our case, due to the continuing laser irradiation during most of the bubble expansion time. The laser energy crossing the bubble and reaching the boundary continues to evaporate water molecules, resulting in an evaporation mass flow $\dot{m}_\mathrm{evap}$[kg/s]. On the other hand, as the bubble grows to a size of several times the fiber diameter, most of the bubble surface is in contact with the cold (close to ambient temperature) water or gel environment. This results in a mass flow $\dot{m}_\mathrm{cond}$ from the vapor phase to the liquid phase due to condensation on the colder parts of the bubble wall.

The local evaporation or condensation rate per unit surface depends on the interface temperature $T_\mathrm{i}(\boldsymbol{r})$ and on the difference between the local vapor density $\varrho_\mathrm{v}(\boldsymbol{r})$ and the equilibrium vapor density $\varrho_\mathrm{v}^\mathrm{e}(T_\mathrm{i})$. The mass flux J[kg m^{-2}s^{-1}] through an interface between a liquid and its own vapor can be estimated from a kinetic treatment by Plesset [33]:

$$J(\boldsymbol{r}) = \alpha\sqrt{\frac{R_\mathrm{g} T_\mathrm{i}(\boldsymbol{r})}{2\pi m_\mathrm{mol}}}\left(\varrho_\mathrm{v}^\mathrm{e}(T_\mathrm{i}(\boldsymbol{r})) - \varrho_\mathrm{v}(\boldsymbol{r})\right), \tag{3}$$

where $\boldsymbol{r}$ represents locations on the bubble boundary, R_g is the universal gas constant and m_mol is the molar mass [kg/mol]. The constant α is an accommodation coefficient [34] for evaporation and condensation, which accounts for the deviation of real interface properties from the ideal case considered in theory. For a freshly created clean water vapor-liquid interface a value of α close to unity can be assumed during the bubble lifetime of some hundreds of microseconds, as no significant impurities are expected that could perturb the phase transition rate at the water-vapor interface. However the polymer component of PAA-gels is expected to lower the accommodation coefficient as compared to pure water.

The vapor mass change rate $\dot{m}_\mathrm{v}(t)$ is then the integral of J over the bubble surface S:

$$m_\mathrm{v}(t) = \int_{t_0}^{t} \dot{m}_\mathrm{v}(t) = \int_{t_0}^{t}\int_{S} J(\boldsymbol{r},t)\,\mathrm{d}S\,\mathrm{d}t$$
$$= \int_{t_0}^{t}\int_{S} \alpha\sqrt{\frac{R_\mathrm{g}T_\mathrm{i}(\boldsymbol{r},t)}{2\pi m_\mathrm{mol}}}\left(\varrho_\mathrm{v}^\mathrm{e}(T_\mathrm{i}(\boldsymbol{r},t)) - \varrho_\mathrm{v}(\boldsymbol{r},t)\right)\mathrm{d}S\,\mathrm{d}t\,. \tag{4}$$

The time dependent vapor mass $m_\mathrm{v}(t)$ influences the bubble dynamics via the local pressure term p_i in (2), which is a function of m_v.

As PAA-gels have a viscoelastic behavior, they have to be characterized by a loss modulus E'' besides their elastic modulus E'. This results practically in an increase of the viscosity η in (2). Our measurements (Fig. 2, Table 1) have shown that E' increases monotonically as a function of polymer content. Furthermore, within the compression frequency range used in our rheology measurements, all gels show a slight increase in elastic modulus E' towards higher frequencies, whereas the loss modulus E'' peaks at a characteristic frequency for each gel concentration and decreases for higher frequencies. Our results are consistent with hydrogel properties described by Brinker and Scherer [30], who showed a maximum of E'' at a characteristic frequency ω_0 and an increase of E' with frequency that saturates for frequencies $\omega \gg \omega_0$. The maxima in the measured E'' of our PAA-gels show that the ω_0's are within the frequency range covered by our rheology measurements for gels of 70–90 % water contents and at lower frequencies for the softest gels (> 90% water content). The boundary velocities encountered during bubble expansion, and thus the gel compression velocities can be as high as 10 m/s, much higher than the highest possible velocities (40 mm/s) of the rheology system used. However, extrapolating the low velocity results for E'' in the light of the hydrogel properties described above, E'' becomes small.

The last three terms of (2), which correspond to resistive forces, are all larger for gels as compared to water. Consequently, the larger size of the bubble in soft gels has to be attributed to the thermodynamics occurring inside the bubble rather than to mechanical properties of the gels. The larger vapor volume obtained could be the result of two effects:

(1) The increased resistance of the gel could delay the bubble formation, resulting in a higher fluence threshold and a stronger superheating of a larger liquid volume before phase change sets in. A more explosive vaporization would consequently create higher initial vapor pressure and thus stronger acceleration, resulting in a larger kinetic energy transfer to the gel around the bubble and consequently in a larger final cavity extension.

(2) Condensation efficiency at the bubble boundary could be lowered by PAA-gels. As a consequence of the lower condensation rate, a longer lived vapor cavity containing a larger vapor mass mv would be created, that would expand to a larger maximal volume.

Our measurements of bubble formation fluence threshold (Fig. 6) have shown no anomalies for soft gels. The bubble formation threshold increases continuously from pure water to gels of increasing stiffness. Consequently, the hypothesis of much stronger initial superheating, causing more rapid bubble expansion, is unlikely.

Thus condensation processes at the bubble boundary seem to be the key element in understanding the observed process. Indeed the maximum volume of the vapor bubble is determined by the initial number of water molecules transferred to the gas phase by the laser induced vaporization process and by the rate of vapor condensation $\dot{m}_\mathrm{cond}$ at the colder parts of the bubble boundary. As can be seen from (3) and (4), the mass flux per unit surface J is essentially a function of the density difference from equilibrium, of the interface temperature and of an accommodation coefficient α of the interface, which is essentially material dependent.

A smaller accommodation coefficient at the PAA-gel surface α_PAA as compared to a water surface $\alpha_{\mathrm{H_2O}}$ will lead to a reduced condensation rate and thus according to the equation of motion (2) to a larger maximal bubble size as well as longer lived bubbles.

Because of these effects, although a larger bubble is formed in soft PAA-gels, a weaker collapse process would be induced, as a slower drop of pressure inside the bubble means less acceleration of the surrounding liquid towards the center. This is consistent with our observation of weaker pressure transients in soft gels than in water (Fig. 9) in spite of larger bubble size (Fig. 5) and longer lifetime (Fig. 10).

The same hypothesis can also explain the generally smaller volume of the bubbles created with the same energy at the tip of the smaller fiber (Fig. 8). The bubbles created with the 600 μm fibers are almost spherical. In contrast, the bubbles induced by the higher fluence reached at the tip of the 400 μm fibers are elongated, and more elliptical in shape. In this case, the ratio of surface to volume is larger than for a sphere. This means that the mass loss by condensation at the boundary is more important relative to the total vapor mass, and consequently the maximum bubble volume is smaller in spite of absorption of the same amount of laser energy.

Comparison with previous data [19], obtained for Q-switched holmium laser pulses of 500 ns duration delivered in PAA-gels and water further supports our explanation. In this case the whole laser energy is deposited in a very short time compared to the bubble lifetime. The bubble dynamics is dominated by the kinetic energy transferred to the surrounding medium in the initial stage of bubble formation under high thermoelastic pressure [19] and subsequent rapid expansion. Evaporation and condensation processes should have a minor influence, compared to the present long pulse induced bubbles. Indeed, the bubbles generated in 5% water content PAA-gel by Q-switched holmium laser pulses were found to be of smaller or equal size than in water [19].

Implications about damage risks during ablation of soft tissue through fibers inserted into the tissue can be drawn from our results. In soft tissue, according to the size of the bubbles generated within the softer gels, tissue damage several millimeters deep can be induced by tissue tearing during the fast (> 10 m/s) bubble formation and expansion phase. Moreover, as water in the vapor phase inside the bubble is almost transparent to 2.12 μm radiation [35], enhanced forward extension of the laser induced tissue alteration can be expected due to the free light path through the transient bubble formed at the delivery fiber tip (Moses effect). This effect might explain the recent observations [36, 37] of heat penetration in intervertebral discs at distances from the fiber tip much

larger than the optical $1/e$ penetration depth of approximately 400 μm.

The pressure transients generated at the bubble collapse are potentially harmful because they can penetrate far deeper into tissue than the laser light. In general, materials are more sensitive to tensile than to compressive stress. In our case, the pressure transients are almost purely compressive with a weak rarefaction tail (Fig. 7), in contrast to the bipolar pressure transients induced by short pulse laser irradiation at an air-tissue interface [38, 39] or at a fiber tip in absorbing liquid [40]. So far, no general pressure amplitude threshold for damage of biological tissue by pressure transients of short (ns range) duration has been established. Available results from literature suggest that besides the pressure amplitude, the number of pressure pulses applied [41] and the stress gradient [9] play a role in tissue damage on a sub-cellular level.

In a recent study by our group on holmium laser ablation of cartilage [42], no indication of a larger range of pressure induced damage in comparison to thermal damage was observed in spite of pressure amplitudes of up to 250 bars at the border of the thermal coagulation zone. In an experiment on mouse breast sarcoma cells in culture, a statistically significant decrease of cell vitality was only observed for peak pressures above 200 bars [9]. In comparison to these results, the relatively modest pressures on the order of 10–100 bars at 3 mm distance due to free running holmium laser pulses measured in this study and the absence of tensile stress suggest that the risks of pressure induced damage are limited to the immediate vicinity of the fiber tip, at least as long as the number of laser pulses delivered is not excessive. For stiffer tissue, damage, if produced, would most likely result from tissue tearing by the bubble expansion, as the maximal pressure observed at the bubble collapse is significantly reduced compared to water.

The mechanical properties of intervertebral discs suggest that transient bubble formation is very likely during laser ablation of the relatively soft inner part of the disk (nucleus pulposus, Table 2). This might lead again to a deeper effective penetration of laser radiation than expected from the absorption coefficient. This risk should be taken into account when estimating minimal safe distances to sensible surrounding structures like nerves.

Another obvious field of significance for our results is fiber-based holmium laser surgery in the vitreous body of the eye, such as cutting of collagenous strands of membranes [4, 43]. Reports of retinal damage at distances of up to 2 mm from the fiber tip [43] can be explained by the effects of transient vapor bubbles. Because the vitreous is a very soft gelled material, special attention should be paid to the size of bubbles, that might even exceed that observed in water, in analogy to our observations in soft PAA-gels.

The results presented above suggest several approaches to reduce the risk of damage due to bubble formation in medical applications like vertebral disc surgery and eye surgery inside the vitreous body. Damage can be diminished by reducing the fluence to the lowest value inducing the desired ablative effect. Bubble size and collapse pressure decrease with fluence for a given fiber diameter. Damage induced by bubbles can be diminished as well by reducing the fiber diameter and maintaining the total pulse energy. The reduction of the fiber diameter decreases mainly the lateral bubble extension, but also the total bubble volume and the pressure transient amplitude.

4 Conclusions

We have shown that transient vapor bubble formation occurs during pulsed holmium laser irradiation of 250 μs duration via optical fibers inside absorbing soft tissue phantoms.

These bubbles generate pressure transients at their collapse inside the phantoms. The effect of fluence, fiber diameter and elastic properties on transient vapor bubble dynamics and pressure transient generation has been systematically studied over a large range of elastic modulus values. Tearing and disruption by the rapid bubble expansion and collapse as far away as several millimeters from the irradiated zone were found as the main risks of mechanical damage. The amplitude of the observed pressure transients was sufficiently low to anticipate only limited damage risks, restricted to delicate tissue structures in close proximity.

Furthermore, our results and the qualitative analysis of the equations governing the bubble dynamics suggest that the rate of vapor condensation at the bubble boundary, plays a central role in the dynamics of bubbles induced by holmium laser pulses.

Acknowledgements. We wish to thank P. Sunderland of the Composite and Polymer Technology Laboratory, Ecole Polytechnique Fédérale de Lausanne, Switzerland, for the access to the rheology equipment and for interesting discussions on mechanical properties of polymers. Our thanks to J.T. Walsh of Northwestern University, Evanston, USA for reading the manuscript and helpful comments and discussions. We also thank K. Rink for helpful discussions and R.P. Salathé for his support. We greatly acknowledge the support from the Swiss optics priority program "Optical Sciences, Applications and Technologies", the Albert and Clemmie Caster Foundation and the office of Naval Research (grant N00014-91-J-1564).

References

1. A.J. Welch, M. Motamedi, S. Rastegar, G.L. LeCarpentier, D. Jansen: Photochem. Photobiol. **53**, 815 (1991)
2. C. Gottlob, G.E. Kopchok, S.K. Peng, M. Tabbara, D. Carvaye, R.A. White: Lasers Surg. Med. **12**, 86 (1992)
3. M. Buchelt, H.P. Kutschera, T. Katterschafka, H. Kiss, B. Schneider, R. Ulrich: Lasers Surg. Med. **12**, 375 (1992)
4. S. Schründer, M. Foerster, N. Müller-Stolzenburg, S. Sola, I. Schmitt, G. Müller: Lasers in Ophthalmology II, Lille, Proc. SPIE **2330**, 39 (1994)
5. W.D. Knopf, K.L. Parr, J.W. Moses, P.E. Cundey, M.D. Cohen, O. Topaz, E. de Marchena, P.Y. Lai, P.B. Kurnik, D.R. Murphy: Circulation **86(I)**, 511 (1992)
6. T.G. van Leeuwen, L. van Erven, J.H. Meertens, M. Motamedi, M.J. Post, C. Borst: J. Am. Coll. Cardiol. **19**, 1610 (1992)
7. F. Könz, M. Frenz, H. Pratisto, H.P. Weber, H. Lubatschowski, O. Kermani, W. Ertmer, H.J. Altermatt, T. Schaffner: Budapest, Proc. SPIE **2077**, 78 (1993)
8. A.G. Doukas, D.J. McAuliffe, T.J. Flotte: Ultrasound Med. Biol. **19**, 137 (1993)
9. A.G. Doukas, D.J. McAuliffe, S. Lee, V. Venugopalan, T.J. Flotte: Ultrasound Med. Biol. **21**, 961 (1995)
10. K. Rink, G. Delacrétaz, R.P. Salathé: Appl. Phys. Lett. **61**, 258 (1992)
11. K. Rink, G. Delacrétaz, R.P. Salathé: Lasers Surg. Med. **16**, 134 (1995)
12. T. Sedlacek, M.A. Martinelli, L. Esterowitz, J.F. Pinto: Proc. SPIE **1646**, 302 (1992)
13. T. Asshauer, K. Rink, G. Delacrétaz: J. Appl. Phys. **76**, 5007 (1994)
14. T. Asshauer, E.D. Jansen, M. Frenz, G. Delacrétaz, A.J. Welch: Laser Interaction with Hard and Soft Tissue II, Lille, Proc. SPIE **2323**, 117 (1994)

15. F. Könz, M. Frenz, H. Pratisto, H.P. Weber, A.S. Silenok, V.I. Konov: Laser-Tissue Interaction II, Barcelona, Proc. SPIE **2624**, 67 (1995)
16. T.G. van Leeuwen, M.J. van der Veen, R.M. Verdaasdonk, C. Borst: Lasers Surg. Med. **11**, 26 (1991)
17. K. Rink, G. Delacrétaz, R.P. Salathé: Appl. Phys. Lett. **61**, 2644 (1992)
18. A. Vogel, S. Busch, M. Asiyo-Vogel: Ophthalmic Technologies III, Proc. SPIE **1877**, (1993)
19. E.D. Jansen, T. Asshauer, M. Frenz, M. Motamedi, G. Delacrétaz, A.J. Welch: Lasers Surg. Med. **18**, 278 (1996)
20. O.M. Lord Rayleigh: Phil. Mag. Ser. **34**, 94 (1917)
21. R. Hickling, M.S. Plesset: Phys. Fluids **7**, 7 (1964)
22. M.S. Plesset: Philos. Trans. Roy. Soc. London A **260**, 241 (1966)
23. G.L. LeCarpentier, M. Motamedi, L.P. McMath, S. Rastegar, A.J. Welch: IEEE Trans. Biomed. Eng. **40(2)**, 188 (1993)
24. M.G. Bini, A. Ignesti, L. Millanta, R. Olmi, N. Rubino, R. Vanni: IEEE Trans. Biomed. Eng. **31**, 317 (1984)
25. L.G. Davis: *Methods in Molecular Biology* (Elsevier, Salem, MA 1986)
26. Y. Li, T. Tanaka, in *Polymer Gels*, edited by D. De Rossi, p. 41 (Plenum, New York 1991)
27. T. Tanaka, S. Ishikawa, I. Coe: Phys. Rev. Lett. **38**, 771 (1977)
28. R.W. Whorlow: *Rheological Technology* (Ellis & Horwood, 1980)
29. H.G. Elias: *An Introdution to Plastics* (VCH, Weinheim 1993)
30. C.J. Brinker, G.W. Scherer: *Sol-Gel Science* (Academic Press, Boston 1990)
31. A. Vogel, W. Lauterborn: J. Acoust. Soc. Am. **84**, 719 (1988)
32. T. Asshauer, K. Rink, G.P. Delacrétaz, R.P. Salathé, B. Gerber, M. Frenz, H. Pratisto, M. Ith, V. Romano, H.P. Weber: Laser-Tissue Interaction V, Los Angeles, Proc. SPIE **2134A**, 423 (1994)
33. M.S. Plesset, A. Prosperetti: Ann. Rev. Fluid Mech. **9**, 145 (1977)
34. E.H. Kennard: *Kinetic Theory of Gases* (McGraw-Hill, New York 1938)
35. P.J. Wyatt, V.R. Stull, G.N. Plass: Appl. Opt. **3**, 229 (1964)
36. M. Buchelt, B. Schlangmann, S. Schmolke, W. Siebert: Lasers Surg. Med. **16**, 179 (1995)
37. K. Zweifel: personal communication (Balgrist Clinic, Zürich 1995)
38. R.O. Esenaliev, A.A. Oraevsky, V.S. Letokhov, A.A. Karabutov, T.V. Malinsky: Lasers Surg. Med. **13**, 470 (1993)
39. G. Paltauf, H. Schmidt-Kloiber: Budapest, Proc. SPIE **2077**, 171 (1993)
40. M. Frenz, G. Paltauf, H. Schmidt-Kloiber: Phys. Rev. Lett. **76**, 3546 (1996)
41. S. Gambihler, M. Delius, W. Brendel: Ultrasound Med Biol **16**, 587 (1990)
42. T. Asshauer, T. Oberthür, T. Jansen, B.E. Gerber, G. Delacrétaz: Laser-Tissue Interaction II, Barcelona, Proc. SPIE **2624**, 49 (1996)
43. S. Borirakchanyavat, C.A. Puliafito, G.H. Kliman, T.I. Margolis, E.L. Galler: Arch. Ophthalmol. **109**, 1605 (1991)
44. A.J. Grodzinsky: CRC Crit. Rev. Biomed. Eng. **9**, 133 (1983)
45. V.K. Goel, J.N. Weinstein: *Biomechanics of the Spine: Clinical and Surgical Perspective* (CRC Press, 1990)
46. F.A. Duck: *Physical Properties of Tissue* (Academic Press, London 1990)